Molecular dynamics study of a solvation motor in a Lennard-Jones solvent

Ken Tokunaga [*]
Division of Liberal Arts, Center for Promotion of Higher Education, Kogakuin University, Nakano machi 2665-1, Hachioji, Tokyo 192-0015, Japan

Ryo Akiyama [†]
Department of Chemistry, Graduate School of Science, Kyushu University, Motooka 744, Nishi-ku, Fukuoka 819-0395, Japan

(Received 6 July 2019; published 30 December 2019)

The motions of a solvation motor in a Lennard-Jones solvent were calculated by using molecular dynamics simulation. The results were analyzed considering the large spatial scale effects caused by the motion of the solvation motor. A reaction site was located on the surface of the solvation motor and the attraction between the reaction site and the solvent molecules was varied for 100 fs. The motion of the motor was driven by solvation changes near the reaction site on the motor. Two finite-size effects were observed in the motion. One was the hydrodynamic effect and the other was the increase in solvent viscosity caused by heat generation. The latter affected not only the displacement of the motor caused by the reaction but also the wave propagation phenomena. Both effects reduced the motor displacement. Heat generation affects the displacement, in particular for small systems. By contrast, the hydrodynamic effect remained even for large systems. An extrapolation method was proposed for the displacement.

DOI: 10.1103/PhysRevE.100.062608

I. INTRODUCTION

When a long-range flow is induced by motion of a colloidal particle, the flow causes other particles to move. This hydrodynamic interaction, which is a long-range effective interaction, plays important roles in particle aggregation, gel formation, and phase separation [1–7]. Simulations for active matters considering the hydrodynamic interaction are also performed [2–7]. In the calculation, hydrodynamics equations, such as the Naiver-Stokes equation, with the implicit solvent model have been often adopted, because calculations for the explicit solvent model are expensive for simulating the collective motions of self-propelled particles.

Before discussing the collective motion of macroparticles, it is not easy to simulate the motion of only one macromolecule in a liquid phase using molecular dynamics (MD) simulations because of the hydrodynamic effects [8–13]. Even if the explicit solvent model is adopted, the ensemble of solvent molecules behaves like a fluid and the motion of a colloidal particle induces a long-range collective motion as the average. That is, hydrodynamic effects become important when we calculate dynamic properties using MD simulation. The effects are long range, as indicated. Therefore, the finite-system-size effect cannot be ignored in MD simulations. The effects on the dynamic properties cannot be removed even if the periodic boundary condition, which can remove the effects from the various static properties, is adopted.

It has been shown that the finite-system-size effect on the calculation for diffusion coefficient is serious [8,10–12,14]. Various diffusion coefficients have been obtained from the velocity autocorrelation functions or gradients of mean-squared displacements based on the calculated MD results. The coefficients become larger as the system size increases. Because of the long-range hydrodynamic effect, the values do not converge when the volume dependence is examined. Theoretical approaches without MD simulations are proposed to avoid this difficulty. There are several theoretical studies for obtaining the diffusion coefficient of a macromolecule in explicit solvent molecules [15–17]. However, the appropriate estimation method based on the simulations becomes more important for comparison between the theoretical and the simulation results.

Fushiki [10] pointed out the above difficulty in the calculation of diffusion coefficient using MD simulation and proposed a method using the linear-response theory and linearized hydrodynamics. We analyzed one of our calculations [14] based on this method and the difference between the coefficients is remarkable. For example, for the finite system of 4000 particles, the estimated diffusion coefficient of a macroparticle for an infinite system is larger by a factor of 1.23 than the calculated one. This difference corresponds to the difference between monomer and dimer if the Stokes-Einstein law is applied.

We have studied the motion of a macroparticle driven by solvation change by using MD simulation with an explicit solvent model [14,18]. This self-propelled particle, *solvation motor*, has a reaction site on the surface and the particle is immersed in the solvent (Fig. 1). The interaction between the reaction site and the solvent molecules is varied for

[*]tokunaga@cc.kogakuin.ac.jp
[†]rakiyama@chem.kyushu-univ.jp

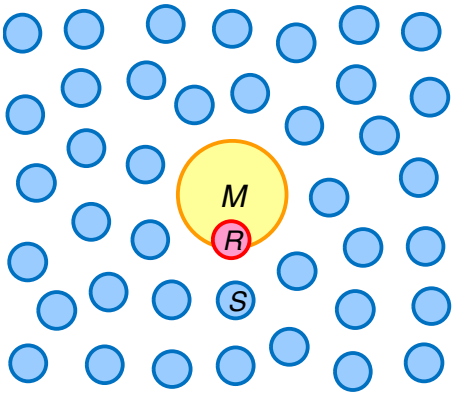

FIG. 1. A solvation motor (MR) in a solvent (S). The solvation motor is composed of a motor part (M) and a reaction site (R).

10–500 fs. This interaction change induces an asymmetric solvation change and the motor molecule moves. This motor molecule motion cannot escape from the finite-size effect caused by the hydrodynamic effect either.

Changes in the solvation structure around the particle [19] and in solvent viscosity by chemical reaction or laser beam [20,21] also affect the individual and collective motions of self-propelled particles. The motions of self-propelled particles with molecular size are strongly affected by the thermal fluctuation, so that the individual and the collective motions are random. To understand the motions, an analysis based on the average over many trajectories is therefore important.

In this article, a method is proposed to estimate the displacement of the motor molecule in an infinite system. We also analyze and discuss other behaviors of the motor and solvent molecules. The discussions are important in simulations of the self-propelled particle with an explicit solvent model.

II. MODEL AND METHODS

We examine a simple system composed of a motor molecule (MR) and solvent (S) particles. The motor molecule has a motor part (M) and a reaction site (R). The R–S and S–S interactions are described by the 6-12 Lennard-Jones (LJ) potential:

$$U_{\mathrm{LJ}}(r_{ij}) = 4\varepsilon_{ij}\left[\left(\frac{\sigma_{ij}}{r_{ij}}\right)^{12} - \left(\frac{\sigma_{ij}}{r_{ij}}\right)^{6}\right], \tag{1}$$

and the $M-S$ interaction is described by the Kihara potential [22]:

$$U_K(r_{ij}) = 4\varepsilon_{ij}\left[\left(\frac{\sigma_{ij}-c}{r_{ij}-c}\right)^{12} - \left(\frac{\sigma_{ij}-c}{r_{ij}-c}\right)^{6}\right], \tag{2}$$

where r_{ij}, σ_{ij}, and ε_{ij} are the distance between particles i and j, the distance at which $U(r_{ij}) = 0$, and the depth of the well, respectively. The core parameter c of the Kihara potential was set to 2.8 Å. The molecular axis is defined as the $R \to M$ direction at the beginning of the reaction ($t = 0$) and is fixed thereafter. The displacement of the center of mass of the motor molecule along the molecular axis is discussed. When the motor molecule moves in the $R \to M$ direction, the displacement is positive.

The size of S (σ_{SS}) was determined to be 2.8 Å to give a packing fraction of $\phi = 0.383$, which is almost the same as the value for water when $\rho_m = 1.0\mathrm{g/cm}^3$. The size of M (σ_{MM}) is three times larger than that of S, $\sigma_{\mathrm{MM}} = 3\sigma_{\mathrm{SS}} = 8.4$ Å, which is almost similar to those of small peptide or of fullerene. The size of R (σ_{RR}) is set as 2.8 Å. The distance between the centers of M and R is 3.4 Å. The surface of R sticks out from that of M by 0.6 Å. We set the masses of these particles as $m_R = m_S = 3 \times 10^{-26}$ kg and $m_M = 26m_R$. The summation of m_M and m_R is equal to $3^3 m_S$ because we assume that the mass is proportional to the volume, and the total volume of M and R is almost equal to 3^3 times the solvent volume. The interaction parameters of M, R, and S are set as $\varepsilon_{\mathrm{MM}} = \varepsilon_{\mathrm{RR}} = \varepsilon_{\mathrm{SS}} = 0.6517$ kJ/mol $= 1.082 \times 10^{-21}$ J [23]. These parameters ε correspond to an uncharged extended simple point charge (SPC/E) model of water [24]. The LJ parameters between different kinds of particles are determined as:

$$\sigma_{ij} = \frac{\sigma_{ii} + \sigma_{jj}}{2}, \quad \varepsilon_{ij} = \sqrt{\varepsilon_{ii}\,\varepsilon_{jj}}, \tag{3}$$

where $i, j = M$, R, and S.

In this study, only the R–S interaction was changed from $\varepsilon_{\mathrm{RS}}$ to $\varepsilon'_{\mathrm{RS}} = 10^3\ \varepsilon_{\mathrm{RS}}$. During the "chemical" reaction time (Δt_R), the R–S interaction parameter is $\varepsilon'_{\mathrm{RS}}$. After the reaction time, $\varepsilon'_{\mathrm{RS}}$ returns to $\varepsilon_{\mathrm{RS}}$. The S–S and S–M interactions do not change before, during, or after the reaction. The R–M intramolecular interaction was ignored in this model; thus, the parameter $\varepsilon_{\mathrm{RM}}$ was set as 0.

In our previous work [18], the change in total energy of the system due to the chemical reaction for $\Delta t_R = 10$ fs and $\varepsilon'_{\mathrm{RS}} = 10^3\ \varepsilon_{\mathrm{RS}}$ was found to be about 1×10^{-18} J, which is several times the reorganization energy of the solvent around a protein in the experiment, $1 \times 10^{-19} - 3 \times 10^{-19}$ J [25–29]. We also found that the displacement of the solvation motor reaches a maximum when $\Delta t_R = 100$ and 200 fs. The main discussion of this work is on the dependence of the displacement of the solvation motor on the size of the system, so that the reaction time Δt_R was set at 100 fs to give the largest displacement. To discuss the system-size dependence for calculations of diffusion coefficient and average displacement, the number of particles ($M + R + S$) was varied to $N = 256$, 500, 864, 1372, 2048, 4000, 6912, 8788, 13 500, and 19 652. The average displacement of a larger system, $N = 32\,000$, was additionally calculated for comparison with that of the infinite system. The system size was set so that the number density (weight density) of the solvent was $\rho_n = 33.33\mathrm{nm}^{-3}$ ($\rho_m = 1.0\,\mathrm{g/cm}^3$). Periodic boundary conditions were applied. The MD simulation period after the beginning of the reaction was 35 ps.

The MD simulations were performed using the velocity Verlet integration algorithm [30] with a time step of 0.5 fs. The M–R length was constrained using the RATTLE method [31]. The S–S interactions over $2.5\sigma_{\mathrm{SS}} = 7.0$ Å were neglected. The simulations before the reaction were carried out with the Nosé-Hoover thermostat [32,33] at a constant temperature, $T = 300$ K. The initial conditions for the following processes were prepared in these canonical ensembles (also called NVT) calculations. After the beginning of the reaction period, however, the simulations were carried out in microcanonical (also called NVE) conditions.

The diffusion coefficient and displacement by the reaction were calculated for each trajectory. The diffusion coefficients of the solvation motor were calculated by integration of the velocity autocorrelation function [34,35] between $t = 0$ and 25 ps. The values were averaged over three dimensions because the solvation motor is almost spherical. The displacement of the solvation motor was defined as the difference between positions along the molecular axis at $t = 0$ and $t = 35$ ps. Then the values of the diffusion coefficient and displacement were averaged over 5000 trials, respectively. The error bars in the figures were obtained from the standard deviation, the number of trials (5000), and the multiplier (1.96) for the 95% confidence interval. The fitting line and curve in figures were obtained by the least-squares fit of samples, considering error bars. Standard errors are also shown.

Fushiki [10] proposed a method to estimate the self-diffusion coefficient of a tagged molecule in a solution using the linear-response theory and linearized hydrodynamics. In the method, the diffusion coefficient in the infinite system is estimated by using the system-size dependence of the diffusion coefficient. Here the radius of a system, r_0, is defined as follows:

$$r_0 = \left(\frac{3V}{4\pi}\right)^{\frac{1}{3}}, \tag{4}$$

where V is the system volume. The system-size dependence of the diffusion coefficient as a function of a/r_0 sits on a straight line, where a is the radius of a hard sphere. The extrapolation value at $a/r_0 = 0$ is the diffusion coefficient in an infinite system.

The diffusion coefficient is

$$D = \frac{k_B T}{\gamma}, \tag{5}$$

where k_B, T, and γ are the Boltzmann constant, temperature, and the friction for the solvation motor MR in the solvent, respectively. Here, the solvation motor is almost spherical. If we assume the Einstein-Stokes law is valid, then the friction γ is $6\pi\eta a'$ under the stick condition, where η and a' are the viscosity of the solvent and the hydrodynamic radius of the solvation motor, MR, respectively [36]. Because of solvation effect, the hydrodynamic radius a' is not always $\sigma_{\mathrm{MM}}/2$. The difference often becomes remarkable because of the solute-solvent interaction and/or effects of additives [15–17].

Here the average trajectory of the solvation motor MR as a function of time can be obtained by MD simulation. The average trajectory asymptotically approaches a value $\langle x_\infty \rangle$ and is defined as the displacement, i.e., the average trajectory $\langle x(t) \rangle$ at $t = \infty$. Because the average external force is zero after the reaction time, the equation of motion of the solvation motor MR is

$$m\langle \ddot{x} \rangle + \gamma \langle \dot{x} \rangle = 0, \tag{6}$$

where m, $\langle x(t) \rangle$, and γ are the mass of the solvation motor MR, the average trajectory, and the friction, respectively. The solution is

$$\langle x(t) \rangle = -v_0 \frac{m}{\gamma} \exp\left[-\frac{\gamma}{m} t\right] + v_0 \frac{m}{\gamma}, \tag{7}$$

where the initial velocity and position are v_0 and 0, respectively. The average displacement $\langle x(t) \rangle$ approaches to $\langle x_\infty \rangle = v_0 m/\gamma$, which is the second term on the right-hand side of Eq. (7), at $t = \infty$.

III. RESULTS AND DISCUSSION

The system-size dependence of the diffusion coefficients of a solvation motor MR with no chemical reaction is shown in Fig. 2. The plotted diffusion coefficients actually sit on a straight line. Therefore, Fushiki's theory is satisfied in the estimation of diffusion coefficient for this system. Figure 2 also shows the importance of this system size analysis in the calculation of the diffusion coefficient. The coefficients for the largest system ($N = 19\,652$) and for the smallest system ($N = 256$) are about 90% and 55%, respectively, of that for an infinite system, $(6.3 \pm 0.1) \times 10^{-9}$ m^2/s. This difference in the diffusion coefficient is very large when we discuss the solvation effect based on Eq. (5) because the magnitude of the finite-system-size effect is comparable to that of the solvation effect [15–17,38–40].

MD simulations for the solvation motor MR with chemical reaction were performed. Figure 3(a) shows 10 motion trajectories of the solvation motor. Before the reaction at $t = 0$, the motor motions are Brownian and no directional motions are observed. Just after the reaction, the motor molecule moves forward; however, each of the trajectories after $t = 10$ ps resembles a random walk. Then the motor molecules move both forward and back. These behaviors mean that the thermal motion of the solvent molecules strongly disturbs the motion of the motor.

Figure 3(b) shows the motion plots of the motor along the molecular axis averaged over 5000 trajectories of the center of mass of the motor molecule, $\langle x(t) \rangle$. The shape of the average trajectory as a function of time is similar to the

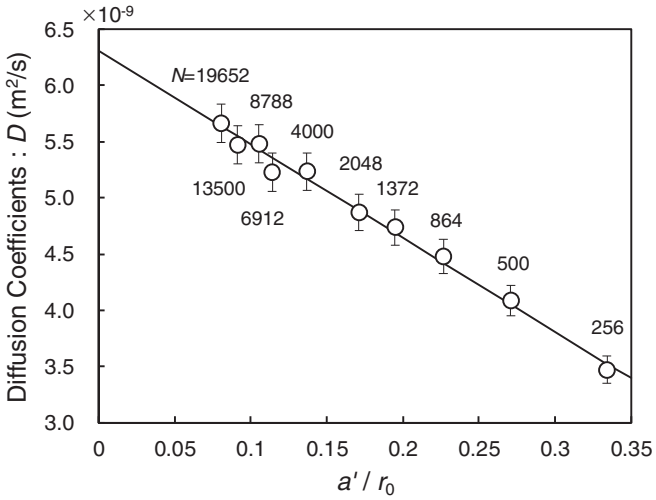

FIG. 2. The diffusion coefficient of the solvation motor MR along the molecular axis as a function of system size a'/r_0 [14,37]. The R–S interactions do not change in this calculation. Circles are average MD simulation results of 5000 trials and the straight line is the least-squares fit of the results. The equation of the line is $D = (-8.3 \pm 0.3)(a'/r_0) + (6.3 \pm 0.1)$.

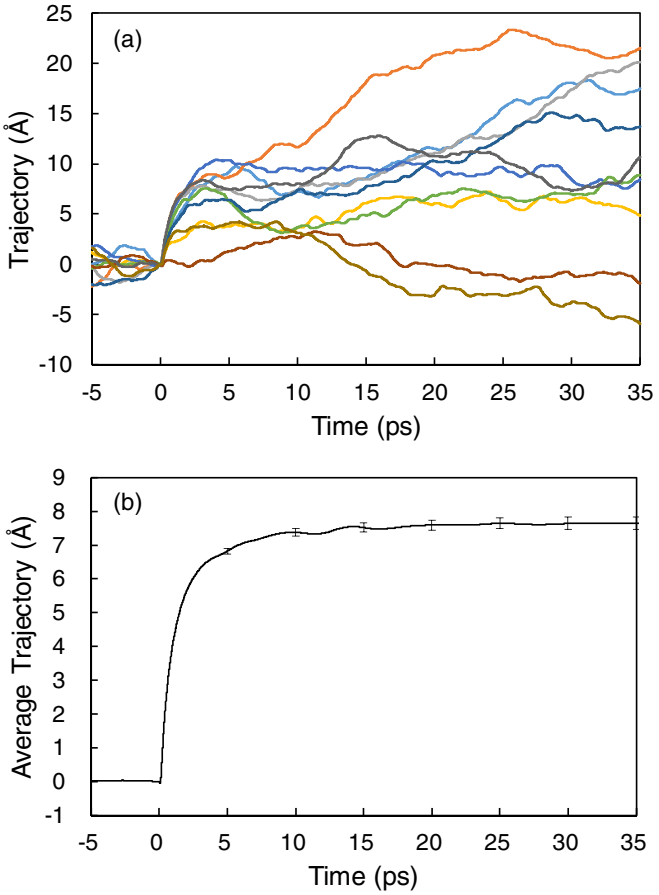

FIG. 3. Motion of the solvation motor *MR* along molecular axis with $N = 19\,652$ plotted as a function of time. (a) Ten trajectories of the solvation motor. (b) Motion of the solvation motor averaged over 5000 trajectories.

solution [Eq. (7)] of the equation of motion. The average displacement $\langle x_\infty \rangle$ is defined as the position at $t = \infty$ but is actually estimated as the position at 35 ps because the average motion of the solvation motor *MR* is stopped by the solvent molecules.

Figure 4 shows the dependence of the velocities of the solvation motor on system size. The solvation motor moves backward at first so that its velocity is negative [18]. Then the velocity turns to positive and reaches the maximum value, about 7.7×10^2 m/s, at 0.17 ps. It is remarkable that before the velocity of solvation motor reaches a peak, the system-size dependence is not observed. The acceleration of solvation motor is due to the collision and dispersion of solvent molecules near the reaction site [18], so that the driving force is independent of system size. By contrast, the velocity of the solvation motor after the peak depends on system size. In other words, the average displacement depends on the system size after the maximum velocity but does not depend on the system size before the maximum velocity. A smaller system size leads to faster relaxation of the motion of the solvation motor.

Figure 5 shows the dependence of the displacement of the solvation motor *MR* on system size a'/r_0. The average displacement before the maximum velocity (Fig. 4) is

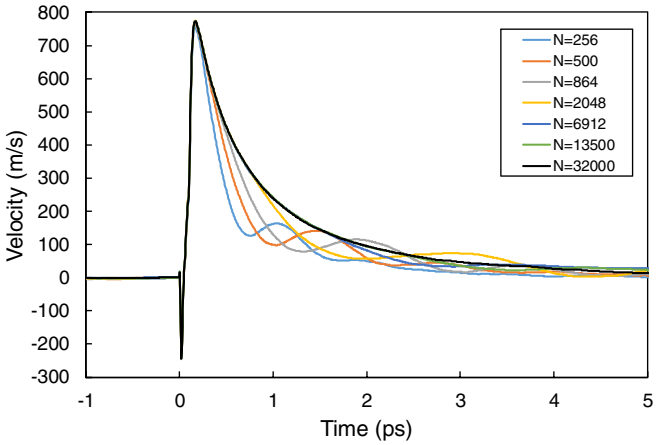

FIG. 4. Dependence of velocities along the molecular axis of the solvation motor on system size. The reaction period is $t = 0-0.1$ ps.

reached, does not depend on system size and the value is about 0.45 Å. The values are 11% and 6% of average displacement for $N = 256$ and $N = 32\,000$, respectively. Substituting $\gamma = v_0 m/\langle x_\infty \rangle$ into Eq. (5) yields the next relation:

$$\langle x_\infty \rangle = \frac{v_0 m}{k_B T} D. \tag{8}$$

If we assume smaller system-size dependencies for T and v_0, then we can expect a linear relationship between displacement $\langle x_\infty \rangle$ and D. When there is a linear relationship, the displacement as a function of a'/r_0 sits on a straight line. The straight blue dotted line is obtained using six points, $N = 864$, 1372, 2048, 4000, 6912, and 8788, as in our previous analysis [14] based on Fushiki's method [10]. If this dotted line is adopted, then the displacement for the infinite system is 8.8 Å. However, in large and small systems, there is a large deviation from the linear fit (dotted line). It seems that this behavior is

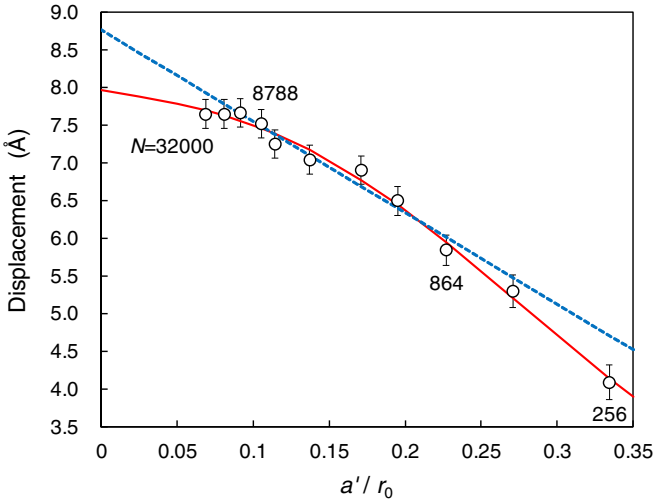

FIG. 5. System-size dependence of the solvation motor *MR* displacement as a function of system size a'/r_0. Circles are 5000 MD trials averages. The blue dotted line is the linear fit of six points ($N = 864-8788$) [14]. The red solid curve was obtained by the least-squares fit of all 11 results for Eq. (14).

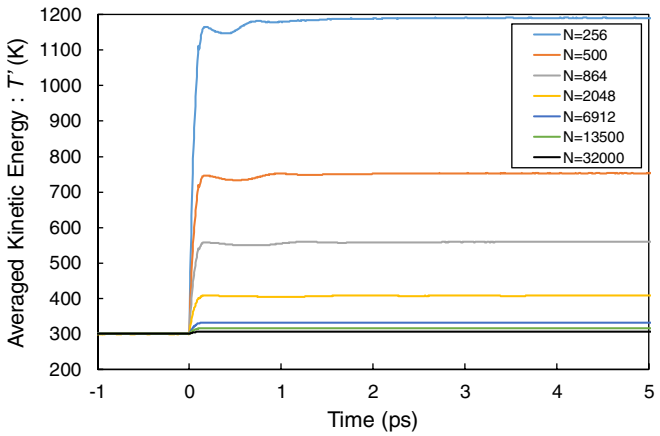

FIG. 6. Dependence of the system's averaged kinetic energy T' on system size. Before ($t < 0$), during ($0 \leqslant t \leqslant 0.1$ ps), and after ($t > 0.1$ ps) the chemical reaction.

caused by the increase in kinetic energy of solvent particles. Next, we will discuss the behavior of the solvation motor considering the increase in kinetic energy.

Figure 6 shows the time change of the averaged kinetic energy of the system. It was found that this energy largely increased by the chemical reaction. In Fig. 6, the averaged kinetic energy was converted to the pseudotemperature T', which is not the thermodynamic temperature [41], because the system is not in equilibrium due to the flow and heat generation. The kinetic energy of solvent molecules around the reaction site was much larger than that of bulk. When the system reached equilibrium after the chemical reaction, its properties would be consistent with those of the temperature, but it takes a long time to reach equilibrium.

The average displacement of the solvation motor is expressed as $\langle x_\infty \rangle = v_0 m/\gamma$. Assuming that v_0 is equal to the maximum velocity of the solvation motor, v_0 is independent of system size (Fig. 4). By contrast, the friction γ has a finite-size effect as

$$\frac{1}{\gamma} = \frac{1}{\gamma_\infty}\left[1 - A\left(\frac{a'}{r_0}\right)\right], \tag{9}$$

where γ_∞ is friction in an infinite system and A is a constant [42,43]. To estimate the diffusion coefficient in an infinite system, a similar relation was also adopted in Ref. [11]. Assuming the Einstein-Stokes law, the friction in an infinite system γ_∞ is written as

$$\gamma_\infty = 6\pi\eta a', \tag{10}$$

where η is the viscosity of solvent molecules. The viscosity is independent of system size at a constant temperature [11]. In the present simulation, however, the kinetic energy of the solvents was increased by the reaction. The increase in equilibrium temperature, ΔT, by the reaction is inversely proportional to the system volume because the increase in kinetic energy of the system is independent of the system size:

$$\Delta T = B\left(\frac{a'}{r_0}\right)^3, \tag{11}$$

TABLE I. Values of fit parameters obtained by the fit of Eq. (14) for the average displacements of 11 finite systems in Fig. 5

Parameters	A'	B'	C'
Values	7.5 ± 0.2	-3 ± 2	20 ± 5

where B is a constant. Based on the Green-Kubo formula [34,35], the viscosity is proportional to the temperature; therefore, using Eq. (11), the system-size dependence of the viscosity after reaction is expressed as:

$$\eta = \eta_0 + C\,\Delta T = \eta_0 + BC\left(\frac{a'}{r_0}\right)^3, \tag{12}$$

where η_0 is viscosity at 300 K before the reaction and C is a constant. Summarizing these formulas, the system-size dependence of the average displacement $\langle x_\infty \rangle$ is obtained as:

$$\langle x_\infty \rangle = \frac{v_0 m}{\gamma} = \frac{\frac{v_0 m}{6\pi\eta_0 a'}\left[1 - A\left(\frac{a'}{r_0}\right)\right]}{1 + \frac{BC}{\eta_0}\left(\frac{a'}{r_0}\right)^3}. \tag{13}$$

The part of the displacement before the maximum velocity that is not dependent on system size was discussed earlier. Equation (13) does not contain the part that is not dependent on system size. Therefore, considering also the part that is not dependent on system size (0.45 Å), the average displacement is rewritten in simple form as:

$$\langle x_\infty \rangle = \frac{A' + B'\left(\frac{a'}{r_0}\right)}{1 + C'\left(\frac{a'}{r_0}\right)^3} + 0.45, \tag{14}$$

where A', B', and C' are constants. In large systems (small a'/r_0), the average displacement $\langle x_\infty \rangle$ would be on a straight line because the hydrodynamic effect is dominant. In small systems (large a'/r_0), the average displacement $\langle x_\infty \rangle$ would be smaller than the displacement predicted from the straight line because the increase in viscosity (or averaged kinetic energy) is dominant. The solid curve in Fig. 5 is the fit of Eq. (14) for the average displacements of 11 finite systems. The fit parameters are shown in Table I. In large systems, the curve is almost linear and the deviation becomes larger as the system size is reduced. The average displacement in the infinite system was estimated as 8.0 ± 0.2Å from the value at $a'/r_0 = 0$. All 11 points indicate that the estimation for the displacement considering increase in averaged kinetic energy is more reasonable than that based on the linear estimation and the background of the phenomena should be important.

We could clarify the motion of the solvation motor by calculation of 5000 trajectories of finite systems with $256 - 32\,000$ particles. However, even in the largest system, the diffusion coefficient and the displacement (5.7×10^{-9} m^2/s, 7.7 Å) do not correspond to those of the infinite system (6.3×10^{-9} m^2/s, 8.0 Å). Therefore, extrapolation of the curve [Eq. (14)] to $a'/r_0 = 0$ is necessary for the prediction of the motion of solvation motor in the infinite system. Our analysis using extrapolation based on Eq. (14) will be more important in the discussion of the motion of a larger and heavier solvation motor in an infinite system.

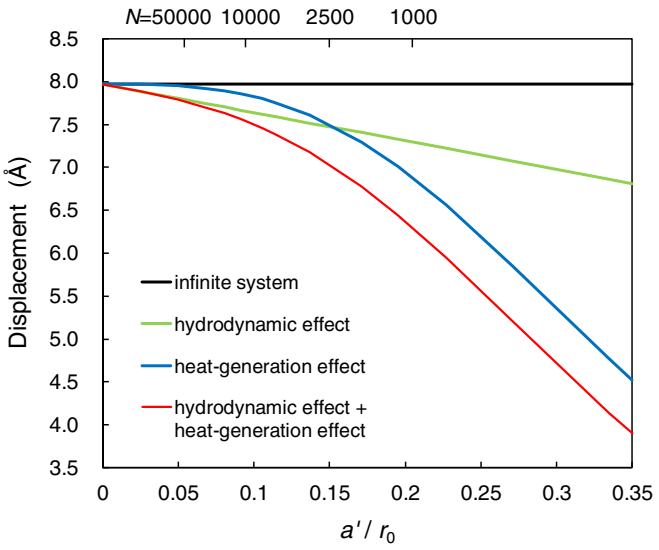

FIG. 7. Contributions of the hydrodynamic and heat-generation effects for the displacement of solvation motor. The black line shows displacement in an infinite system obtained from the fit of 11 finite systems for Eq. (14). The green line shows the system-size dependence of the displacement considering only the hydrodynamic effect, $\langle x_\infty \rangle = A' + B'(a'/r_0) + 0.45$. The blue curve shows the system-size dependence of the displacement considering only the heat-generation effect, $\langle x_\infty \rangle = A'/[1 + C'(a'/r_0)^3] + 0.45$. The red curve shows displacement considering both effects, Eq. (14). This curve was shown in Fig. 5. The values $A' = 7.5$, $B' = -3$, and $C' = 20$ shown in Table I were adopted.

The large spatial scale effect for the displacement of the solvation motor is divided into contributions of the hydrodynamic and heat-generation effects (Fig. 7). When $N > 50\,000$, the heat-generation effect is very small and negligible, but the hydrodynamic effect is dominant. The heat-generation effect starts to appear at $10\,000 < N < 50\,000$, but the hydrodynamic effect is still dominant. The contributions of the hydrodynamic and heat-generation effects are comparable in $1000 < N < 10\,000$. The heat-generation effect surpasses the hydrodynamic effect during this N range. In small systems ($N < 1000$), the heat-generation effect is much larger than the hydrodynamic effect. To summarize the above, the motion of the solvation motor is mainly affected by the hydrodynamic effect in large systems ($N > 10\,000$) and by the heat-generation effect in small systems ($N < 1000$).

The oscillatory behavior of the motor motions observed in Figs. 3(b) and 4 seems to be due to the finite size of the system. At first, we fitted Eq. (7) to the average trajectory by simulation [Fig. 3(b)]. Next, we took the difference between the trajectories obtained by simulation and by the fitting. Then, Fourier transform (FT) of the difference was performed to extract the frequencies of the solvation motor motion for $N = 4000-19\,652$ (Fig. 8). There were three or four peaks (shown by arrows and marks) of frequency that shifted to a lower frequency as the system size increased. The small difference between the positions of the sine and cosine peaks would be due to the motion of the solvation motor itself.

Figure 9 shows the frequency and period of the peaks in Fig. 8. The solid straight lines are least-squares fits for the

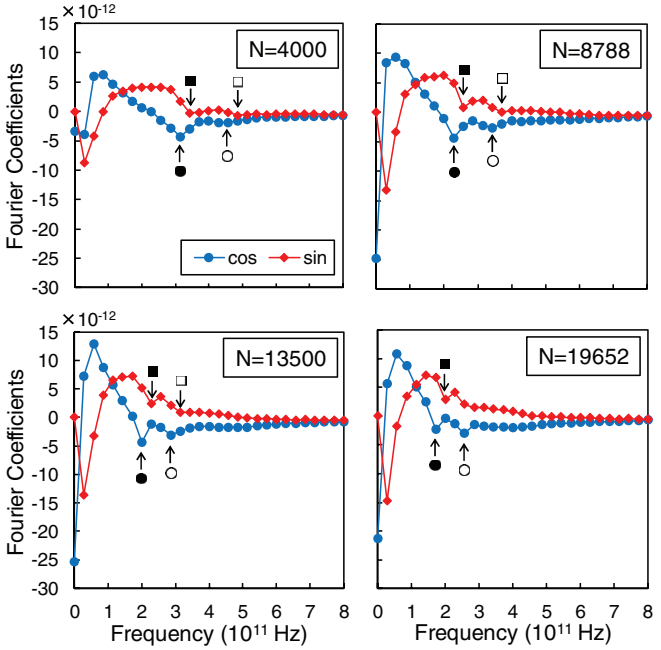

FIG. 8. Fourier coefficients of the motion of the solvation motor for $N = 4000$, 8788, 13 500, and 19 652.

peaks of the Fourier coefficients. The frequency approaches 0 when the system size becomes infinite and the period of the wave also approaches 0 when the system size becomes 0, so that these peaks were due to the periodic boundary condition and the finite size of the system.

Figure 10(a) shows the velocities of fast and slow (acoustic) waves estimated from Fig. 9. The velocity of the acoustic wave was $1.5 - 1.7 \times 10^3$ m/s, which was near that of liquid water at room temperature, about 1.5×10^3 m/s [44]. During the chemical reaction period, solvent molecules approach the reaction site due to the attraction between the solvent molecules and the reaction site [18]. This acoustic wave originated from the dispersion of solvent particles that were attracted close to the reaction site into the bulk after the

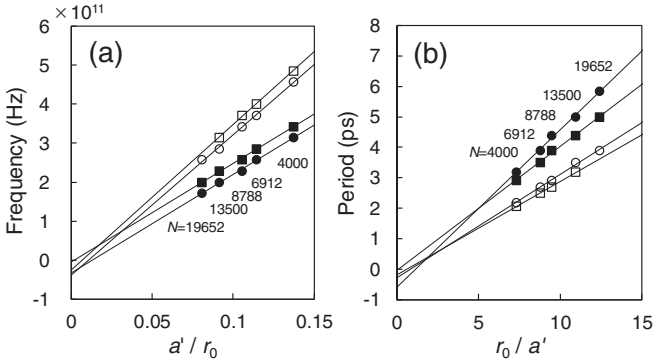

FIG. 9. System-size dependence of (a) frequency and (b) period of peaks obtained by FT of the difference between simulation and Eq. (7) with $N = 4000-19\,652$. Circles and squares mean cosine and sine components, respectively. Marks in these figures correspond to those in Fig. 8.

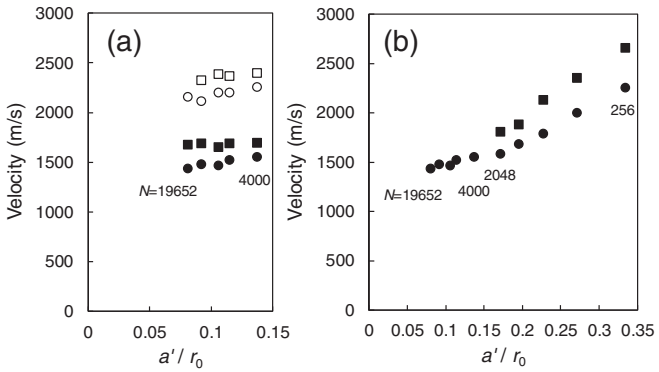

FIG. 10. Velocity of waves obtained by FT of (a) coordinate and (b) velocity of solvation motor. Marks in (a) correspond to those in Figs. 8 and 9.

reaction period. The oscillatory behavior of the motor motion is mainly due to this acoustic wave.

The origin of the slow wave was confirmed by the following procedure. In the system with $N = 8788$, the motor was fixed during and after the reaction ($t = 0-5$ ps), after which it was made to be free to move after $t = 5$ ps. Therefore, only the backward wave from the motor is induced in this simulation. After $t = 5$ ps the motor slowly moved backward with the oscillation. The period of oscillation was 4 ps, which is same as that of the slow wave in Fig. 9(b). This result means that the wave induced by the dispersion of solvents near the reaction site corresponded to the slow acoustic wave through the system.

The velocity of the fast wave was $2.2 - 2.4 \times 10^3$ m/s, which is 7×10^2m/s faster than that of the acoustic wave. Figure 4 shows the average velocity along the molecular axis of MR. The maximum velocity of the solvation motor, 7.7×10^2 m/s, was almost the same as the difference between the velocities of fast and acoustic waves in Fig. 10(a). Therefore, the fast wave will be a shock wave by the forward motion of solvation motor.

A similar procedure was applied to the analysis of the velocity of solvation motor (Fig. 4). The result of $N = 32\,000$ was set as reference; then, we took the difference between the velocity of the other finite systems and that of the reference. Figure 10(b) shows the velocities of waves obtained by FT of the difference.

There are three interesting findings. The first one is that the FT of coordinates [Fig. 10(a)] gives peaks in large–middle-size systems ($N = 19\,652-4000$), but the FT of velocities [Fig. 10(b)] gives peaks not only in large–middle-size systems, but also in small-size systems ($N \leqslant 2048$). The second one is that the velocity of the waves increases as the system size decreases [Fig. 10(b)]. This is because the increase in the averaged kinetic energy becomes larger as the system size decreases (Fig. 6). The velocities of slow waves in $N = 19\,652-4000$ of Fig. 10(b) are consistent with those of Fig. 10(a), so that Fig. 10(b) complements the small-size system region of Fig. 10(a). The last one is that fast shock waves are observed in Fig. 10(a) but not in Fig. 10(b). The increase in averaged kinetic energy is very large in small systems, so that the velocity of shock wave becomes very fast (short period). Additionally, a shock wave disperses and interferes with itself in small systems. Therefore, fast waves are invisible in small systems.

IV. CONCLUSION

We have investigated the system-size dependence of the motion of a solvation motor composed of LJ particles. A linear relationship was observed between the system size (a'/r_0) and diffusion coefficients (D). The value of D of an infinite system was estimated as 6.3×10^{-9} m^2/s by extrapolation of the straight line. By contrast, the average displacement $\langle x_\infty \rangle$ was not located on the straight line because of increase in the averaged kinetic energy by the reaction. Considering the change in viscosity due to the increase in averaged kinetic energy, $\langle x_\infty \rangle$ of the infinite system was estimated as 8.0 Å. For a larger and heavier solvation motor, our analysis based on Eq. (14) will play a more important role for the motion prediction in an infinite system. Last, we found by using FT that the oscillation of a solvation motor was due to the acoustic wave traveling backward of the motor and the shock wave traveling forward of the motor.

ACKNOWLEDGMENTS

The authors thank Prof. A. Yoshimori, Dr. Y. Nakamura, and Dr. Y. Uematsu for their comments. This work was supported by Japan Society for the Promotion of Science (JSPS) KAKENHI Grants No. JP19H01863, No. JP19K03772, No. JP18H03673, No. JP18K03555, No. JP17K14550, No. JP16K05512, and No. JP15K05249. The computations were mainly performed using the computer facilities at the Research Institute for Information Technology (Kyushu University, Japan) and the Research Center for Computational Science (Okazaki, Japan).

[1] U. Khadka, V. Holubec, H. Yang, and F. Cichos, Nat. Commun. **9**, 3864 (2018).
[2] P. S. Mahapatra and S. Mathew, Phys. Rev. E **99**, 012609 (2019).
[3] J. R. Villanueva-Valencia, J. Santana-Solano, E. Sarmiento-Gómez, S. Herrera-Velarde, J. L. Arauz-Lara, and R. Castañeda-Priego, Phys. Rev. E **98**, 062605 (2018).
[4] A. Barbot and T. Araki, Soft Matter **13**, 5911 (2017).
[5] S. K. Schnyder, J. J. Molina, Y. Tanaka, and R. Yamamoto, Sci. Rep. **7**, 5163 (2017).
[6] N. Yoshinaga and T. B. Liverpool, Phys. Rev. E **96**, 020603(R) (2017).
[7] I. Buttinoni, J. Bialké, F. Kümmel, H. Löwen, C. Bechinger, and T. Speck, Phys. Rev. Lett. **110**, 238301 (2013).
[8] B. J. Alder, D. M. Gass, and T. E. Wainwright, J. Chem. Phys. **53**, 3813 (1970).

[9] J. J. Erpenbeck and W. W. Wood, Phys. Rev. A **43**, 4254 (1991).
[10] M. Fushiki, Phys. Rev. E **68**, 021203 (2003).
[11] I. C. Yeh and H. Hummer, J. Phys. Chem. B **108**, 15873 (2004).
[12] R. O. Sokolovskii, M. Thachuk, and G. N. Patey, J. Chem. Phys. **125**, 204502 (2006).
[13] Y. Ishii and N. Ohtori, Phys. Rev. E **93**, 050104(R) (2016).
[14] K. Tokunaga and R. Akiyama, J. Comput. Chem. Jpn. **17**, 80 (2018).
[15] Y. Nakamura, A. Yoshimori, and R. Akiyama, J. Phys. Soc. Jpn. **81**, SA026 (2012).
[16] Y. Nakamura, A. Yoshimori, and R. Akiyama, J. Mol. Liq. **200**, 85 (2014).
[17] Y. Nakamura, A. Yoshimori, and R. Akiyama, J. Phys. Soc. Jpn. **83**, 064601 (2014).
[18] K. Tokunaga and R. Akiyama, J. Phys. Soc. Jpn. **81**, SA019 (2012).
[19] S. Y. Reigh and R. Kapral, Soft Matter **11**, 3149 (2015).
[20] D. Rings, R. Schachoff, M. Selmke, F. Cichos, and K. Kroy, Phys. Rev. Lett. **105**, 090604 (2010).
[21] D. Rings, M. Selmke, F. Cichos, and K. Kroy, Soft Matter **7**, 3441 (2011).
[22] T. Kihara, J. Phys. Soc. Jpn. **6**, 289 (1951).
[23] I. M. Svishchev and P. G. Kusalik, J. Chem. Phys. **99**, 3049 (1993).
[24] H. J. C. Berendsen, J. R. Grigera, and T. P. Straatsma, J. Phys. Chem. **91**, 6269 (1987).
[25] M. R. Gunner and P. L. Dutton, J. Am. Chem. Soc. **111**, 3400 (1989).
[26] J. M. Ortega, P. Mathis, J. C. Williams, and J. P. Allen, Biochemistry **35**, 3354 (1996).
[27] J. P. Allen, J. C. Williams, M. S. Graige, M. L. Paddock, A. Labahn, G. Feher, and M. Y. Okamura, Photosynth. Res. **55**, 227 (1998).
[28] J. Li, E. Takahashi, and M. R. Gunner, Biochemistry **39**, 7445 (2000).
[29] R. Schmid and A. Labahn, J. Phys. Chem. B **104**, 2928 (2000).
[30] W. C. Swope, H. C. Anderson, P. H. Berens, and K. R. Wilson, J. Chem. Phys. **76**, 637 (1982).
[31] H. C. Anderson, J. Comput. Phys. **52**, 24 (1983).
[32] S. Nosé, J. Chem. Phys. **81**, 511 (1984).
[33] W. G. Hoover, Phys. Rev. A **31**, 1695 (1985).
[34] R. Kubo, J. Phys. Soc. Jpn. **12**, 570 (1957).
[35] M. P. Allen and D. J. Tildesley, *Computer Simulation of Liquids* (Oxford University Press, Oxford, 1987).
[36] A. Einstein, Ann. Phys. **322**, 549 (1905).
[37] Values of a'/r_0 were calculated assuming that the hydrodynamic radius a' is equal to $\sigma_{\mathrm{MM}}/2 = 4.2$ Å.
[38] S. Nishida, T. Nada, and Terazima, Biophys. J. **87**, 2663 (2004).
[39] S. Nishida, T. Nada, and Terazima, Biophys. J. **89**, 2004 (2005).
[40] J. S. Khan, Y. Imamoto, M. Harigai, M. Kataoka, and Terazima, Biophys. J. **90**, 3686 (2006).
[41] Solvent molecules around the reaction site have a large kinetic energy during and just after the chemical reaction. The thermodynamic temperature cannot be defined in such a situation. Therefore, the pseudotemperature in this study is defined as the averaged kinetic energy over all solvent molecules.
[42] H. Hasimoto, J. Fluid Mech. **5**, 317 (1959).
[43] F. Orts, G. Ortega, E. M. Garzón, and A. M. Puertas, Comput. Phys. Commun. **236**, 8 (2019).
[44] M. Greenspan and C. E. Tschiegg, J. Res. Natl. Bur. Stand. **59**, 249 (1957).